Adjustments for Wind-Induced Undercatch in Snowfall Measurements based on Precipitation Intensity

Matteo Colli[1,2], Mattia Stagnaro[2,3], Luca Lanza[2,3], Roy Rasmussen[4] and Julie M. Thériault[5]

[1] Electrical, Electronics and Telecommunication Engineering and Naval Architecture Department, University of Genoa, Genoa, 16145, Italy
[2] WMO/CIMO Lead Centre ''B. Castelli'' on Precipitation Intensity, Genoa, 16145, Italy
[3] Department of Civil, Chemical and Environmental Engineering, University of Genoa, Genoa, 16145, Italy
[4] Research applications Laboratory, National Center for Atmospheric Research[*], Boulder, 80307-3000, Colorado, USA
[5] Department of Earth and Atmospheric Sciences, Centre ESCER, Université du Québec à Montréal, Montreal, H2X 3Y7, Quebec, Canada

Correspondence to: Matteo Colli (matteo.colli@unige.it)

Abstract. Adjustments for the wind-induced undercatch of snowfall measurements use transfer functions to account for the expected reduction of the collection efficiency with increasing the wind speed for a particular catching-type gauge. Based on field experiments or numerical simulation, collection efficiency curves as a function of wind speed also involve further explanatory variables such as surface air temperature and/or precipitation type. However, while the wind speed or wind speed and temperature approach is generally effective at reducing the measurement bias, it does not significantly reduce the Root Mean Square Error (RMSE) of the residuals, implying that part of the variance is still unexplained. In this study, we show that using precipitation intensity as the explanatory variable significantly reduces the scatter of the residuals. This is achieved by optimized curve fitting of field measurements from the Marshall field-test site (CO, USA), using a non-gradient optimization algorithm to ensure optimal binning of experimental data. The analysis of a recent quality-controlled dataset from the Solid Precipitation InterComparison Experiment campaign of the World Meteorological Organization confirms the scatter reduction, showing that this approach is suitable to a variety of locations and catching-type gauges. Using Computational Fluid-Dynamics simulations, we demonstrate that the physical basis of the reduction in RMSE is the correlation of precipitation intensity with the particle size distribution. Overall, these findings have the potential to improve operational measurements since improved adjustments only require the use of the wind speed information.

1 Introduction

In-situ liquid and solid precipitation measurements commonly employ catching-type gauges to collect hydrometeors while approaching the ground surface. Factors affecting the capability of the gauge to collect and measure the actual precipitation occurring at a given site include wind, wetting, splashing, etc. (WMO, 2014). For a given gauge, we define the Collection

---

[*] The National Center for Atmospheric Research is sponsored by the National Science Foundation

Efficiency (CE) as the ratio between the precipitation amount P_{meas} (mm) measured by the gauge and the true precipitation P_{true} (mm):

$$CE = \frac{P_{meas}}{P_{true}}$$

In case of analytical or numerical models, the true precipitation is known, while it is generally unknown in the field for real world measurements. In this second case, it is common to replace P_{true} with a reference value P_{ref} obtained from high quality instruments and/or specific installations.

In case of snowfall measurements, wind plays a dominant role in reducing the gauge collection efficiency (Goodison et al., 1998; Rasmussen et al., 2012). Nespor and Sevruk, 1999; Constantinescu et al., 2006 used Computational Fluid-Dynamic (CFD) simulations to evaluate the wind-induced undercatch of rainfall. Thériault et al. (2012) used it for snowfall and compared the results with detailed observations of snow crystals. A recent analysis by Colli et al. (2015) showed good agreement between the collection efficiency predicted by time averaged models of wind speed and particle trajectories and the field observations made at the NCAR/NOAA/FAA Marshall Field Test site (CO, USA, Rasmussen et al. 2012). A shielded gauge in the Double Fence International Reference (DFIR) configuration provided the reference precipitation, since this reference system is designated as the international standard gauge shield configuration for snowfall measurement (Goodison et al. 1998).

Adjustment methodologies (e.g. Yang et al., 1995) have been developed and are typically algebraic relationships between CE and the mean wind speed U_w (m s^{-1}), also referred to as transfer functions. Thériault et al. (2012) and Colli et al. (2015a) specified CE curves as a function of wind speed for different solid precipitation types (following Rasmussen et al., 1999) and particle size distributions (PSD). Wolff et al. (2015) proposed a sigmoidal function for the CE using the observations collected in Haukeliseter (Norway). This relationship includes the air temperature T (°C) as an additional parameter to take into account the likely amount of water contained in the precipitation particles.

Wolff et al. (2015) and Colli et al. (2016b) showed that the influence of the type of precipitation on the catch performance of precipitation gauges could be taken into account by specifying the CE values according to the air temperature when considering the transition from snow to rain. The air temperature is an efficient indicator to determine the type of precipitation such as rainfall ($T>2$°C), wet snow (-2°C$<T<+2$°C) and dry snow ($T<-2$°C). However, this is not representative of the large variety of crystal types and the degree of riming (Rasmussen et al., 1999 and Thériault et al., 2012).

Recently, Kochendorfer et al. (2017a,b) described a simplified inverse exponential formulation for the universal transfer function using wind speed and air temperature. Their analysis is based on measurements collected at the Marshall field site and highlighted that a large Root Mean Square Error (RMSE) still remain even though a transfer function can reduce the gauge's bias to near zero. Thériault et al (2012) suggest using observations and simulations that the RMSE is due to the large variability in the particle type and size distribution of snowfall. The temperature can help determining the phase of the precipitation but not the size of hydrometeors, which helps explain the small impact of air temperature on the RMSE. Large uncertainties are also observed in the DFIR (Thériault et al., 2015) based on CFD simualtions.

Further numerical simulations were conducted to study the fundamental processes leading to the large scatter in the data for a given wind speed. Colli et al. (2015) presented dry snow *CE* estimations for an unshielded and a Single Alter (SA) shielded gauges (Alter, 1934) based on data from the Marshall field site. The comparison of CFD simulations with the observations (Thériault et al., 2012; Colli et al., 2015) showed that a large part of the *CE* variability for a given wind speed is explained by the particle size distribution. Thériault et al. (2012; 2015) reported that the catch performance of a shielded gauge is also related to the particle's fall speed in the vicinity of the gauge.

These studies suggest that the particle type, size and the wind field can affect the gauge collection efficiency. To explore this further, we note that it is possible to represent the size distribution of precipitation particles by an inverse exponential function (Marshall and Palmer, 1948) that depends on two parameters, the slope and the intercept of its logarithmic representation. Pruppacher and Klett (1997) show that the slope of the PSD is closely related to the precipitation rate. As the precipitation rate increases, the slope of the size distribution decreases, leading to a higher concentration of large particles. Previous studies (e.g. Folland, 1988; Nespor and Sevruk, 1998), focusing on liquid precipitation only, specified the functional relationships between wind-induced undercatch and wind for different rainfall rate classes. Therefore, we suggest that the precipitation rate, i.e. snowfall intensity (SI), can be used to improve adjustments based on the *CE* curves. Such possibility is explored in this paper and shows to significantly reduce the RMSE.

Our method of investigation first considers precipitation gauge data collected at the Marshall (CO, USA), CARE (Canada) and Haukeliseter (Norway) field-test sites. Second, using CFD simulations, different PSDs are numerically tested and the *CE* is evaluated based on the associated precipitation intensity. This allowed testing the proposed hypothesis in a simplified environment where the noise that is typical of experimental datasets is avoided. The results show a good agreement of the *CE* values with field data and a clear dependency on the SI.

The measurements and the data processing method used to perform the field data analysis are presented in section 2. Section 3 reports on the observed correlation between *CE* and the measured *SI* or the environmental temperature. A description of the data binning optimization according to *SI* is also included. The influence of the chosen temporal aggregation of measurements on the derived *CE* is described in section 4. In section 5, the dependency between the *CE* and the measured SI is investigated using CFD simulations with the aim of providing a physical basis for the correlation observed in section 3.

2 Methodology of field data analysis

2.1 Field data processing

The development and testing of new methodologies to retrieve the *CE* requires the availability of quality controlled, high frequency meteorological measurements from a properly instrumented test bed. The snowfall measurements used in this study were collected by two weighing gauge systems, one consisting of a Single Alter (SA) shield surrounding a Geonor T200B weighing gauge with a 6-second sampling frequency and the second a DFIR shielded Geonor T200B. Both systems were co-located at the Marshall field site (CO, USA, Rasmussen et al., 2012) during 2013-2015 as part of the Solid Precipitation

InterComparison Experiment program (SPICE) by WMO (Nitu et al., 2018). Ancillary data was also collected at the Marshall Field site every minute to support investigation into factors that might affect the *CE*. The SA Geonor T200B gauge measurements are compared to those made by the DFIR shielded Geonor T200B gauge, which was defined as the working automated reference for WMO-SPICE (Kochendorfer et al., 2017c).

5   Wind speed is measured 2 m above the ground surface using a propeller anemometer (Model 05103 Wind Monitor, RM Young) whereas the temperature was measured 1.5 m above the ground surface using a fan-aspirated (Model 076B Radiation Shield, Met One Instruments) platinum resistance thermometer (Model CS500-L, Campbell Scientific).

Geonor weighing gauges are based on vibrating wire technology. Noise in the output is typically due to environmental factors that cause oscillations of the measuring bucket. These effects have been reduced by post-processing the 6 s raw time series

10   with a Gaussian linear time-invariant filter characterized by a filtering window equal to 2 min and a standard deviation equal to 1 min. A correction of the vibrating wires sensitivity to the environmental temperature has been applied as well. In addition, an automatic quality control was performed to check the occurrence of missing data, decreasing trends or jumps in the precipitation time series and inconsistent data from the three vibrating wires of the Geonor T200B gauge (Reverdin, 2016).

The measured *CE*, already defined in Section 1, is now better specified as the ratio between the precipitation amount measured

15   by the SA shielded gauge (P_{SA}) and the one measured by the DFIR shielded gauge (P_{DFIR}), as follows:

$$CE = \frac{P_{SA}}{P_{DFIR}}$$

As for the Marshall field test site, we focused on the WMO-SPICE 30-min quality controlled site event data sets (SEDS), according to the procedure described in Reverdin (2016) and Kochendorfer et al. (2017b). Only 30-min data with reference precipitation (P_{DFIR}) larger or equal to 0.25 mm were considered, for a total of 72 days of precipitation recorded from October

20   2013 to April 2015. The dataset was further reduced to consider events with an environmental temperature less than -2°C, to avoid the occurrence of liquid precipitation (Colli et a., 2015), resulting in a final dataset of 213 30-min intervals (A-SEDS in Table 1).

The SEDSs from CARE (Canada) and Haukeliseter (Norway) were processed in a similar way and denoted B-SEDS and C-SEDS respectively in Table 1. At the CARE field site, the wind speed and temperature measured at 2-m above ground was

25   measured by a NWS425 anemometer and HMP155 thermometer (Vaisala). At the Haukeliseter field site, wind speed measurements were made at 10 m level above the ground by a WindObserver II anemometer manufactured by Gill Instruments and a PT100 platinum resistance thermometer sensor measured the environmental temperature. We adopted the Kochendorfer et al. (2017a) approach to converting 10-m wind to 2-m gauge height wind. This entails correcting the 10 meter wind by a factor of 0.71; U_{10m} x 0.71, assuming a logarithmic vertical profile of wind speed (Thom, 1975).

30

Table 1: Location, measurement period, time interval and data consistency of SEDS (site event data set) considered in the analysis

Dataset	Location	Period	Time interval	N. of 30-min data
A	Marshall (CO-USA)	Jan. 2013 – Apr. 2015	1 min	6943
A-SEDS	Marshall (CO-USA)	Oct. 2013 – Apr. 2015	30 min	213
B-SEDS	CARE (Canada)	Nov. 2013 – Apr. 2015	30 min	234
C-SEDS	Haukeliseter (Norway)	Nov. 2013 – Apr. 2015	30 min	485

Because the snowfall type, particle size distribution and terminal velocity at a given location are highly variable in time, shorter time intervals were also tested. Most meteorological services (Matrosov et al.,2009; Gergely and Garrett, 2016) use 30-min or 60-min intervals. To investigate the influence of the sampling interval on the *CE* variation with wind speed, the original 1-min dataset from the Marshall test site from January 2013 to April 2015 was aggregated to 5-min, 10-min and 20-min time intervals. The wind speed and temperature datasets were averaged over the same time intervals. A lower snowfall rate measured by the DFIR was set to $SI_{DFIR} = 0.5$ mm/h to avoid cases of very light snow. Under these conditions, the total dataset – indicated as A in Table 1 – is composed of a total of 6943 one-minute samples recorded during 29 different precipitation events.

2.3 Data analysis method

We analyse the *CE* as a function of wind speed and air temperature, as suggested by Wolff et al (2015) and Korchendorfer et al. (2017a), then we investigate the role of SI as an alternative explanatory variable. The SI is linked to the PSD and the vertical velocity of particles by the following equation:

$$SI = \alpha \int_{D_{min}}^{D_{max}} N(D) \cdot w_p(D) \cdot D^3 dD \qquad (1)$$

where *D* is the particle diameter (mm), *N(D)* the number of particles with diameter D, $w_p(D)$ the vertical velocity (m s^{-1}) and α is a factor that accounts for the shape of the snowflakes.

The *CE* function suggested by Korchedoffer et al. (2017a) as a function of wind and the air temperature is expressed as:

$$CE = e^{-a(U_w)\left(1-[\tan^{-1}(b(T))+c]\right)} \qquad (2)$$

where U_w is wind velocity, *T* is the air temperature, while *a*, *b* and *c* are empirical coefficients.

The role of the SI is tested using the following equation:

$$CE = e^{-a(U_w)\left(1-[\tan^{-1}(b(SI))+c]\right)} \qquad (3)$$

where *a*, *b* and *c* are numerical best-fit coefficients. Equation (2) takes into account the precipitation phase while equation (3) takes into account the size of the hydrometeors.

3 Results from the field data analysis

The empirical *CE* for the SA shielded gauge as a function of wind speed is shown in Figure 1 using the 30-min dataset A-SEDS. In the two panels, *CE* data are colour coded according to the air temperature *T* (panel a) and to the snowfall intensity SI_{SA} (panel b). No significant correlation is visually evident in panel a, while panel b shows a distinct cluster of low precipitation rates at low *CE*. While for any given wind speed, different *CE* may occur depending on the SI_{SA}, there is a higher *CE* observed when the gauge collects the higher *SI*. This trend becomes more evident when the mean horizontal wind speed is higher than 2 m/s.
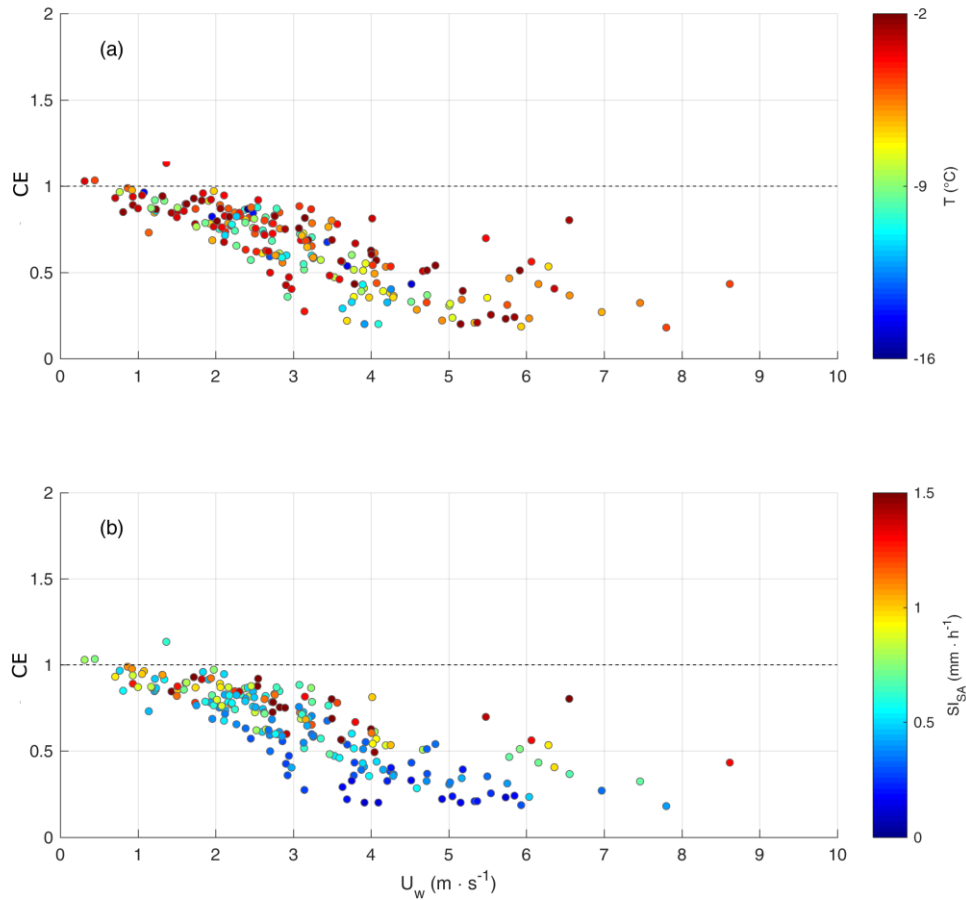
Figure 1: Collection efficiency $CE=P_{SA}/P_{DFIR}$ for the 30 min SA shielded gauge measurements from the Marshall field site in the period October 2013 to April 2015. Data are colour coded according to the air temperature *T* (panel a) and the measured snowfall intensity SI_{SA} (panel b).

One explanation of the larger *CE* is related to larger particle sizes having trajectories that are less prone to deflection by the deformed airflow above the gauge collector (as detailed in Thériault et al., 2012 for different crystal types and by Colli et al. 2016a,b). Colli et al. (2015) showed a correlation between the slope parameter of the *PSD* outside the tested gauge and its *CE* by means of CFD analysis and the results were supported by disdrometers field data. Larger particles are associated with lower slope of the *PSD* and therefore higher *SI* (Pruppacher and Klett, 1997).

A least squares regression was performed on the inverse exponential function of the *CE* based on wind speed and temperature (Eq. 2) and the one based on wind speed and *SI* (Eq. 3). The coefficients obtained from the best-fit analysis are listed in Table 2.

Table 2: Best-fit coefficients a, b and c of the inverse exponential function, number of 30-min intervals used (n) and linear correlation coefficient (R) based on measurements made by the SA shielded gauge at the Marshall (USA), CARE (Canada) and Haukeliseter (Norway) field test sites from October 2013 to April 2015. Coefficients are calculated for both the $CE(U_w, SI_{SA})$ and $CE(U_w, T)$ at each field test site.

Field test site	CE formulation	a	b	c	n	R
Marshall (USA)	$CE(U_w, SI_{SA})$	0.6737	12.8976	0.6589	213	0.91
	$CE(U_w, T)$	0.0520	0.1874	1.4971	213	0.82
CARE (Canada)	$CE(U_w, SI_{SA})$	3.4531	107.4708	0.5835	234	0.85
	$CE(U_w, T)$	0.2892	0.0126	-0.7551	234	0.75
Haukeliseter (Norway)	$CE(U_w, SI_{SA})$	0.4217	7.6856	0.7372	485	0.87
	$CE(U_w, T)$	0.5650	0.0198	-0.6711	485	0.75

The two regressions are presented in Figure 2. These are the $CE(U_w, SI_{SA})$ (panel a) and $CE(U_w, T)$ (panel b) surfaces together with the field measurements (red dots). The *CE* surfaces are colour-coded. The $CE(U_w, SI_{SA})$ regression (panel b) shows a relevant dependency on the measured snowfall intensity. In contrast, the $CE(U_w, T)$ regression represented in panel a shows a weaker dependency to the environmental temperature *T* than with the *SI*.
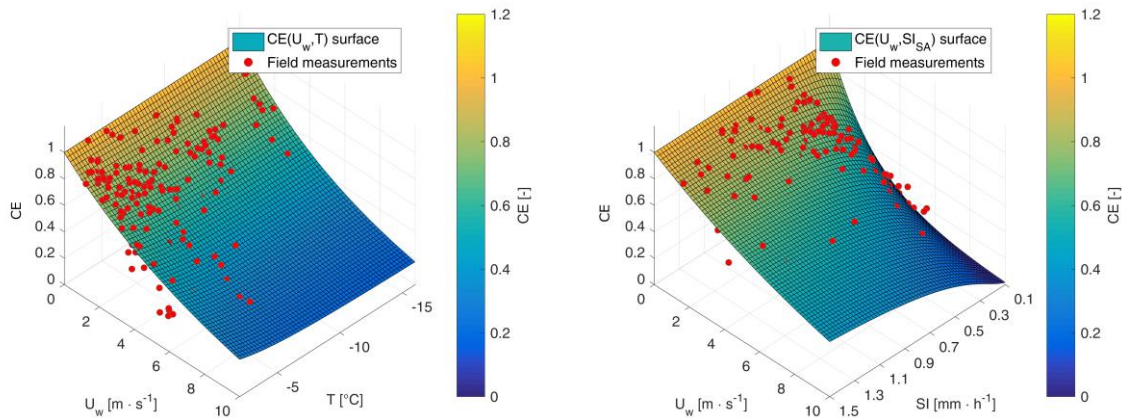
Figure 2: Best-fit *CE* surfaces for the 30-min SA shielded snow gauge measurements made at the Marshall field test site (red dots). Two regressions are shown by expressing *CE* as a function of the wind speed and either the air temperature *T* (panel a) or the measured snowfall intensity *SI*$_{SA}$ (panel b).

To ensure optimal regression of the observed dependency between the *CE* and the *SI* measured by the uncorrected gauge, a

5   non-gradient multi-objective genetic optimization algorithm, implemented in the DAKOTA open source toolkit (Eldred et al.,

2007), was used to retrieve the best *SI* class limits. The following classes were obtained: $0.0 < SI_{SA} <= 0.4$ mm h^{-1}, $0.4 < SI_{SA} <= 0.6$

mm h^{-1}, $0.6 < SI_{SA} <= 1.0$ mm h^{-1} and $1.0 < SI_{SA} <= 1.5$ mm h^{-1}. The optimization objectives were to maintain a significant sample

size for each bin and to minimize the scatter (RMSE) of the residuals. Figure 3 presents $CE(U_w, SI_{SA})$ plots for smaller subsets

of field data according to the optimised *SI* classes. The results show that each intensity category has a different fit to a sigmoid

10   function, with the lowest *SI* class having the steepest decrease in *CE* with increasing wind speed. This is again explained by

the highest intensities being associated with the largest particles, therefore slowly decreasing their *CE* with wind speed.
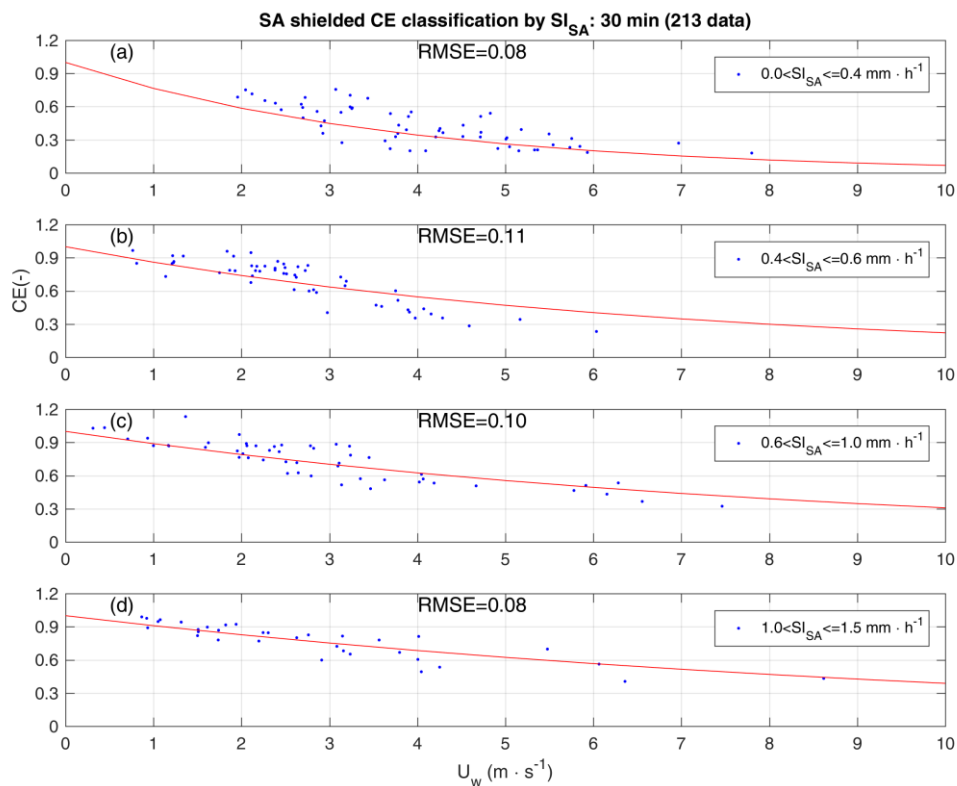
Figure 3: Empirical *CE* for the 30-min SA shielded snow gauge measurements made at the Marshall field test site as a function of
15   **wind speed. The solid line in each panel is the sigmoidal best fit to the data. Each panel represents a different *SI* range as defined in the legends and reports the RMSE of the residuals.**

Figure 4 compares best-fit *CE* curves computed as a function of wind speed and either temperature or the *SI*. It shows that there is evidence of much stronger dependence on the *SI* classification (solid lines) than on temperature (dotted lines). The four *CE(U$_w$,T)* curves (dashed lines) show similar trends and are very close to each other, demonstrating that there is no significant correlation of the *CE* with temperature below -2° C. In contrast, the curves show a distinct separation when categorized by *SI* for the 30-min dataset (solid lines).
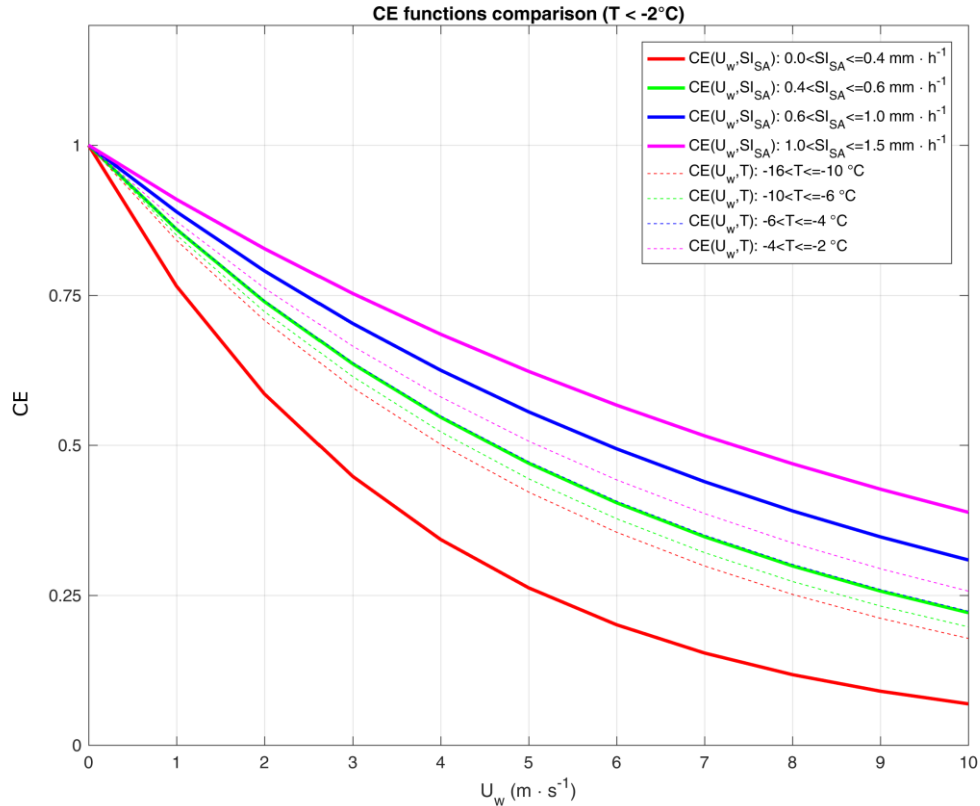
Figure 4: Best-fit *CE* curves of the 30-min measurements made by the SA shielded snow gauge at the Marshall field test site using either the air temperature *T* (dashed lines) or the measured *SI* (solid lines). *SI* curves are the same as in Figure 3.

An evaluation of the improved snowfall accumulation estimates when using the *SI* dependent curve fit is shown in Figure 5a, where the corrected *CE* is shown and the root mean square error (*RMSE*) of the residuals is reported. The residual scattering is quantified by a *RMSE* equal to 0.10 and the colour coded distribution based on the environmental temperature appears quite random. A larger scatter (*RMSE*=0.14) is observed when the measurements are corrected using wind speed and temperature (Figure 5b, traditional approach). Note that Figure 5b shows a colour separated dependence of the residuals on the *SI*, indicating that notwithstanding the *CE(U$_w$,T)* correction some form of dependency persists between the SA shielded gauge undercatch and the characteristics of precipitation.
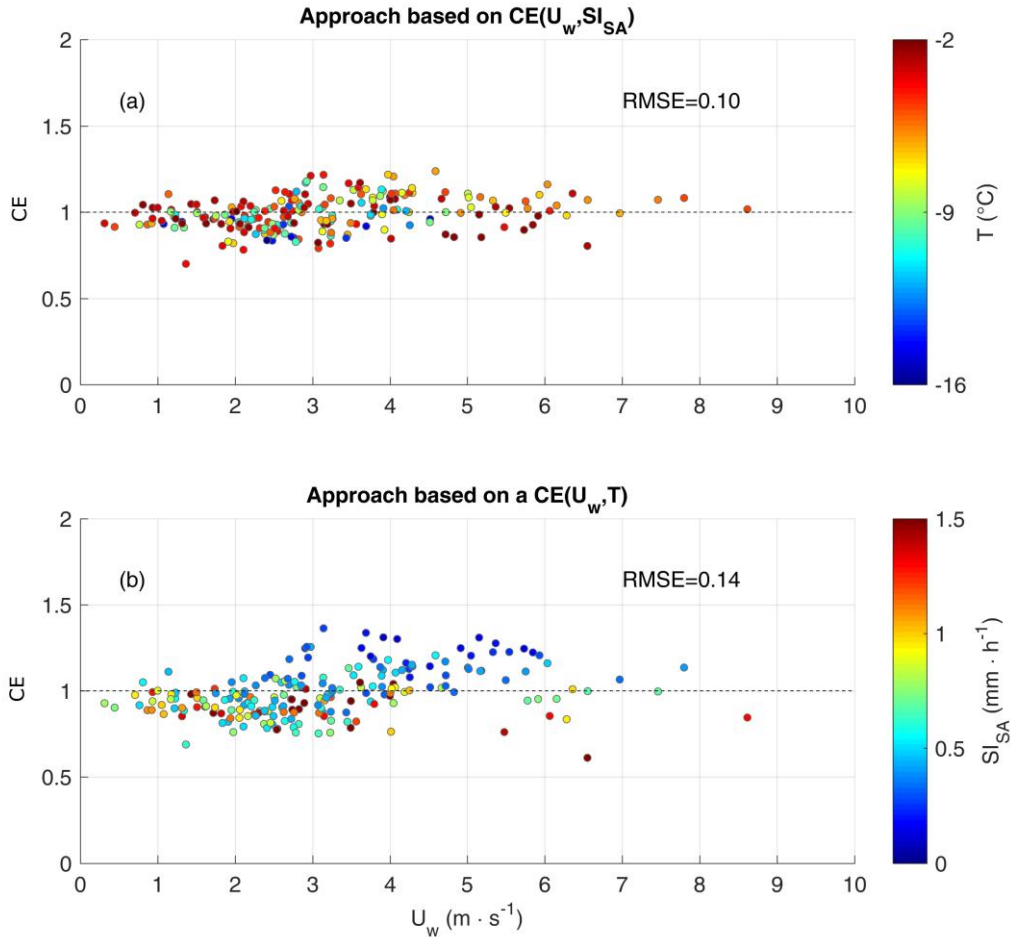
Figure 5: Residuals obtained after correcting the 30-min SA shielded snow gauge measurements from the Marshall field test site using Equation 3 (top panel) and Equation 2 (bottom panel), with the associated RMSE values. Residuals are colour coded according to the environmental temperature T (top panel) and the snowfall intensity SI_{SA} (bottom panel).

The best fit coefficients of the collection efficiency regression obtained with the CARE and Haukeliseter datasets are reported in Table 2 for both the $CE(U_w,T)$ and $CE(U_w,SI_{SA})$ formulations. The correction of the measurements based on such transfer functions is shown in Figures 6 and 7. The RMSEs of the residuals for the CARE measurements are equal to 0.09 in the case of $CE(U_w,SI_{SA})$ and 0.12 in the case of $CE(U_w,T)$ while the residuals for the Haukeliseter measurements show RMSEs that are equal respectively to 0.16 and 0.22. These RMSE results confirm that the approach based on the wind speed and SI leads to an improved correction of the solid precipitation measurements. The results of the field data analysis suggest that the

environmental temperature can be used to provide an approximated criterion to recognize the precipitation phase (liquid, mixed or solid) while the *SI* is a more efficient explanatory variable since it is directly related to the *PSD*.
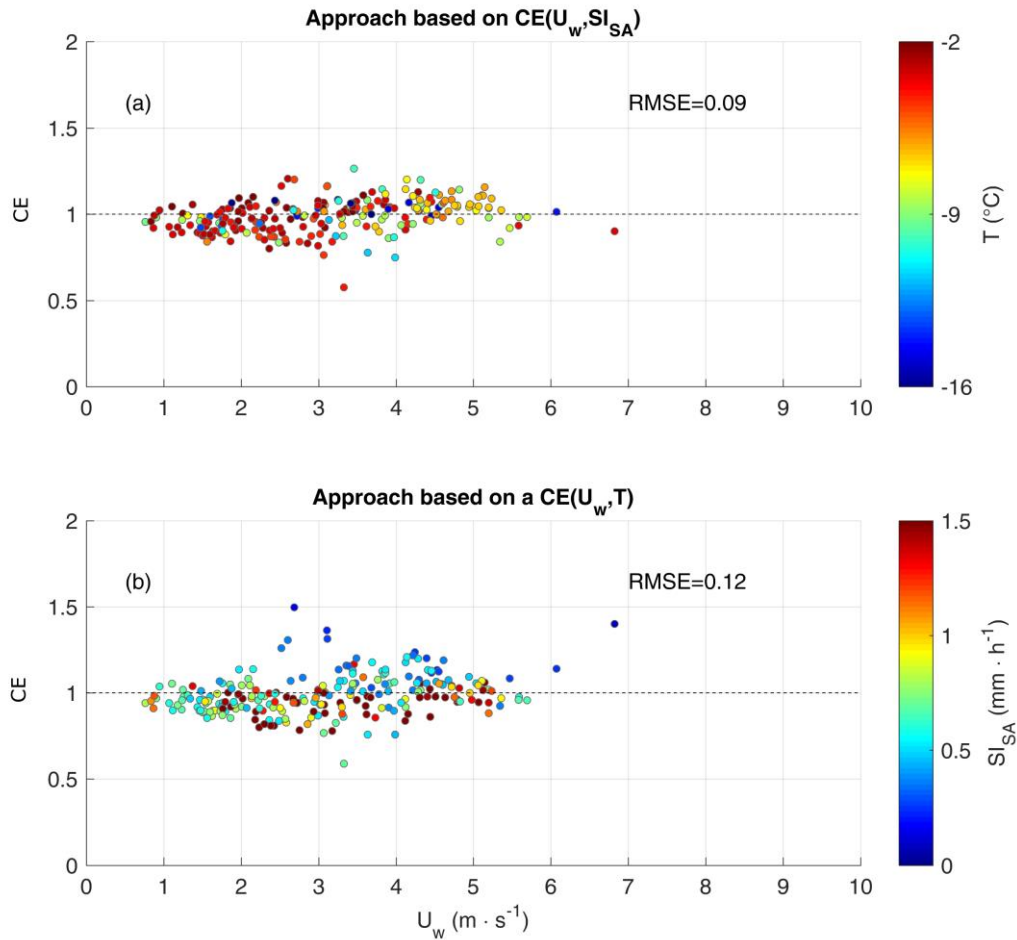
Figure 6: Residuals obtained after correcting the 30-min SA shielded snow gauge measurements from the CARE (Canada) field test site using Equation 3 (top panel) and Equation 2 (bottom panel), with the associated RMSE values. Residuals are colour coded according to the environmental temperature T (top panel) and the snowfall intensity SI_{SA} (bottom panel).
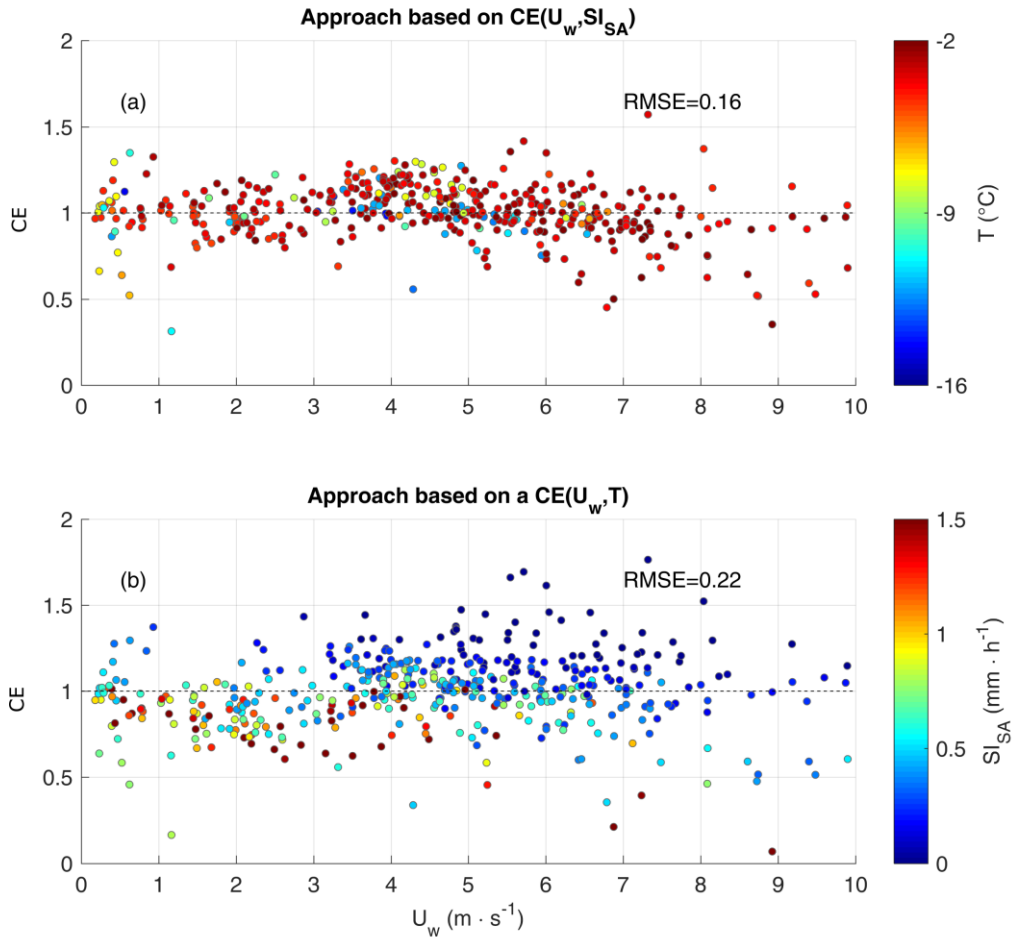
Figure 7: Residuals obtained after correcting the 30-min SA shielded snow gauge measurements from the Haukeliseter (Norway) field test site using Equation 3 (top panel) and Equation 2 (bottom panel), with the associated RMSE values. Residuals are colour coded according to the environmental temperature T (top panel) and the snowfall intensity SI_{SA} (bottom panel).

4 Sensitivity to the time aggregation

The analysis of field data proposed in section 3 has been repeated on the 1-min measurements performed by the SA shielded gauge at the Marshall field test site from January 2013 to April 2015 and aggregated over time intervals equal to 5, 10, 30 and

10   60 min. The regression coefficients obtained by applying the inverse exponential functions described by equations 2 and 3 are reported in Table 3. Figure 8 shows the *CE* curves calculated for different measured snowfall intensities SI_{SA} and time

resolutions Δt. In all cases, a strong CE dependency on SI_{SA} draws distinct variations with wind speed, which do not overlap with each other. On the other hand, measurements made with a 30-min sampling interval provide CE curves that are closer to each other, and hence slightly less influenced by the measured SI, but still significantly different. This is partially explained by the fact that SI_{SA} is strongly aggregation dependent and when the intensity measurements are averaged over a large time interval they become less representative of the internal variability.

The representativeness of the proposed $CE(U_w,T)$ transfer functions (represented by their linear correlation coefficient r in Table 3) with respect to the field measurements decreases sharply below 5 minutes for temperature, while it doesn't for $CE(U_w,SI_{SA})$, suggesting that the T dependence becomes weaker at high resolution while the SI_{SA} dependence not so much. A similar behaviour is reported in Table 4 in terms of $RMSE$, where the transition between the 5-min and the 1-min aggregation intervals yields the larger $RMSE$ increase for the $CE(U_w,T)$ formulation. Therefore, the dependence on SI_{SA} is more robust with respect to time aggregation. As shown in section 3, WMO-SPICE used a 30-min aggregation interval to assess the CE, which still show significant variability at any given wind speed.

Table 3: Coefficients (a, b and c) of the inverse exponential function fitted at various aggregation intervals for the $CE(U_w,T)$ and $CE(U_w,SI_{SA})$ formulations, with the associated linear correlation coefficient (r), and number of data available (n). The calculation used measurements made by the SA shielded gauge at the Marshall field test site from January 2013 to April 2015.

| Δt | $CE(U_w,T)$ | | | r | $CE(U_w,SI_{SA})$ | | | r | n |
| | a | B | c | | a | b | c | | |
(min)	(-)	(-)	(-)		(-)	(-)	(-)		
1	0.0588	0.6575	1.0502	0.60	18.0058	213.0772	0.5717	0.87	6943
5	0.0539	0.7155	1.1036	0.75	1.8436	27.9843	0.5957	0.90	1405
10	0.0500	1.1350	1.1648	0.81	0.4372	6.5754	0.6851	0.91	697
30	0.0555	0.9313	0.8761	0.85	0.3141	4.8702	0.7596	0.94	226
60	0.0539	1.0996	0.9338	0.87	0.2985	4.6410	0.7649	0.95	115
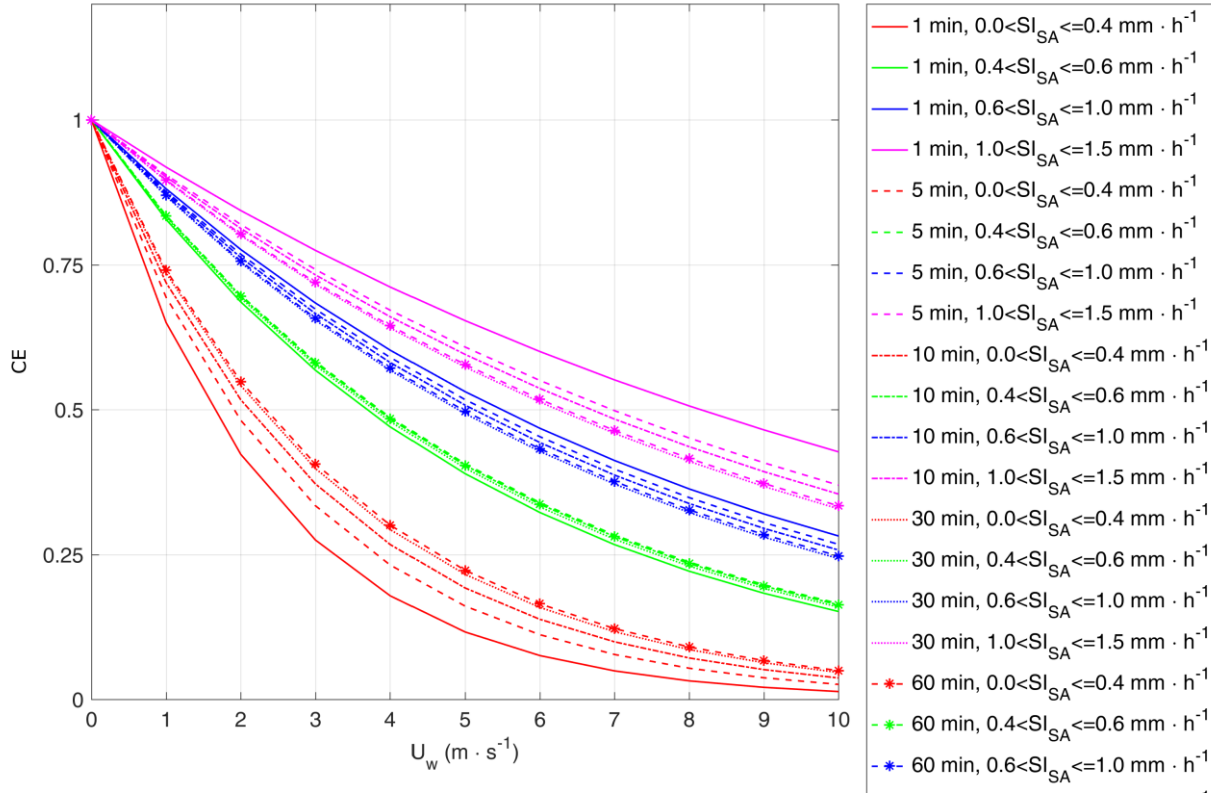
Figure 8: Best-fit *CE(U_w,SI)* curves of the SA shielded snow gauge at the Marshall field site at 1, 5, 10, 30 and 60-min sampling intervals (different line types) grouped by the measured *SI* (different line colors).

5 Figure 8 demonstrates that the 10-min time interval may represent a trade-off point between the availability of correlated SI_{SA} and *CE* observations and the need of aggregating the measurement over a longer interval during low precipitation intensity. An evaluation of the impact of the data integration time on the correction of the P_{SA} observations was made by considering snowfall accumulations computed at different aggregation intervals. Table 4 shows that a larger dispersion of the *CE* of the corrected measurements (quantified by the *RMSE*) around the optimal value (*CE*=1) is observed when short aggregation

10 intervals are considered. Table 4 also shows that smaller *RMSEs* are systematically observed when the *CE* is calculated using the measured *SI*. Indeed, shorter aggregation intervals yield a larger improvement of the correction when using the measured *SI* rather than temperature, as demonstrated by larger values of the difference ΔRMSE=RMSE(*CE(U_w,T)*)-RMSE(*CE(U_w,SI)*).

Table 4: RMSE of precipitation measurements made by the SA shielded gauge at the Marshall field test site over different aggregation intervals Δt after applying the correction based on SI, $CE(U_w, SI_{SA})$, and air temperature, $CE(U_w, T)$, and their difference $\Delta RMSE$.

Δt	RMSE ($CE(U_w, T)$)	RMSE ($CE(U_w, SI_{SA})$)	$\Delta RMSE$
(min)	(-)	(-)	(-)
1	0.26	0.16	0.10
5	0.19	0.12	0.07
10	0.16	0.11	0.05
30	0.13	0.08	0.04
60	0.12	0.07	0.05

The fact that the amount of scatter reduction $\Delta RMSE$ increases with shorter aggregation intervals, seems to support the need of high-resolution measurements to improve the accuracy of the snow data. For instance, the scatter resulting from the correction of 30-min accumulation measurements based on wind speed and temperature can be achieved for 10-min accumulation measurements if the SI is used for the correction. Thus by using the SI in the transfer function instead of temperature, one can either achieve a higher skill for a given aggregation time or achieve a higher aggregation interval with a RMSE similar to the one traditionally obtained for a longer aggregation interval.

5. CFD simulation and validation

The following section presents the CFD modelling framework used to compare to the observations in section 3 and to validate the physical basis of using the SI as an explanatory variable for the CE.

5.1 Airflow modelling and CE calculation

The flow field around a SA shielded gauge was numerically simulated using the Open Foam software and is described by Colli et al. (2015). The time-averaged air velocity, turbulent kinetic energy and pressure fields were solved by means of a Reynolds Averaged Navier-Stokes k-ω SST model.

The trajectories of drysnow particles falling through the CFD flow field are calculated using a Lagrangian model (Colli et al. 2015) for wind speeds between 1 and 8 m/s. The particle characteristics are from Rasmussen et al. (1999).

Several particle sizes were simulated to capture the dependence of CE on particle size. The PSD of snowfall events can be described using the gamma distribution, as shown by Brandes et al. (2007), which is similar than Marshall and Palmer (1948) but with a shape parameter,:

$$N(D) = N_0 \cdot D^{\mu} \cdot D^{-\lambda \cdot D} \tag{4}$$

where D is the snowflake diameter, N_0 is the scale parameter, μ characterizes the curvature and λ the slope of the distribution. According to Brandes et al. (2007) μ can be estimated by the following expression: $\mu=-0.00499\,\lambda^2+0.798\,\lambda-0.666$. In this work we adopted a general intercept value equal to $N_0=1.5\,10^6$ mm^{-1}m^{-3} and, based on observations, the slope parameters used are 0.5 mm^{-1} < λ < 1.5 mm^{-1} (Brandes et al.,2007; Houze et al, 1979). The estimation of CE is based on the particle counting technique described in Colli et al. (2016b), :

$$CE(U_w) = \frac{\int_0^{d_{pmax}} V_w(d_p) A_{inside}(d_p, U_w) N(d_p) d_p}{\int_0^{d_{pmax}} V_w(d_p) A_{gauge} N(d_p) d_p} \tag{5}$$

where $A_{inside}(d_p, U_w)$ is the effective collecting area associated with the number of particles collected by the gauge and $A_{gauge}(dp, U_w)$ is the area associated with the entering particles in the case of undisturbed airflow. Finally, $V_w(d_p)$ is the equivalent water volume.

5.2 PSD and snowfall intensity collected by the gauge

The link between snowfall intensity computed based on the simulation and the slope of the size distribution is given in Table 5. It shows that steeper slopes of the PSD (represented by higher λ), and as a consequence smaller mean particle sizes, are characterized by lower values of the CE. This is due to the stronger influence of the airflow around the gauge collector on the trajectories of the smaller particles. The CE values calculated in Table 5 show that the variability of CE for a given λ remains significant in all the simulations performed with a wind speed higher than 3 m s^{-1}.

Table 5: Ratio between the collected SI and the reference SI by varying the wind speed U_w (m s^{-1}) and the slope parameter λ (mm^{-1}) of the PSD.

λ	0.5	0.7	0.9	1.1	1.3	1.5	1.7	1.9
SI	8.49	3.86	2.1	1.26	0.81	0.54	0.38	0.27
U_w= 1 m/s	1	1	1	1	1	1	1	1
U_w= 2 m/s	0.97	0.97	0.97	0.97	0.97	0.97	0.97	0.97
U_w= 3 m/s	0.94	0.93	0.93	0.93	0.93	0.93	0.93	0.92
U_w= 4 m/s	0.87	0.86	0.85	0.84	0.84	0.83	0.82	0.81
U_w= 5 m/s	0.78	0.74	0.7	0.67	0.63	0.6	0.57	0.54
U_w= 6 m/s	0.69	0.61	0.54	0.47	0.41	0.35	0.31	0.27
U_w= 7 m/s	0.51	0.39	0.29	0.21	0.15	0.11	0.08	0.06
U_w= 8 m/s	0.32	0.19	0.11	0.06	0.03	0.02	0.01	0.01

The CFD analysis performed by Thériault et al. (2012) found that the type of precipitation and their sizes explained some of the scatter in the gauge catch efficiency for a given U_w. Colli et al. (2015) confirmed this conclusion by providing different $CE(U_w)$ functions as well as an improve drag coefficient using the same slope parameters (λ= 0.25, 0.50 and 1 mm^{-1}) as in Thériault et al. (2012).

To link the snowfall intensity with the PSD, an example of the simulated size distribution of dry snow particles that fall into the gauge is shown in Figure 9 for a sample precipitation characterized by λ=1.0 mm^{-1} and N_0=10^6 mm^{-1}m^{-3}. These PSD parameters were suggested by Houze et al. (1979) who observed the snow size distribution in different atmospheric conditions. In agreement with Figure 9 of Thériault et al. (2012), it is shown that the gauge starts missing the lower particle sizes when U_w approaches 4 m s^{-1}, and higher wind speeds correspond to narrower ranges of particle diameters that are collected by the gauge (and higher curvature parameter μ). This smaller particles fall in the gauge at 4 m/s than previously found by Thériault et al. (2012). This is probably due to the updated drag coefficient.
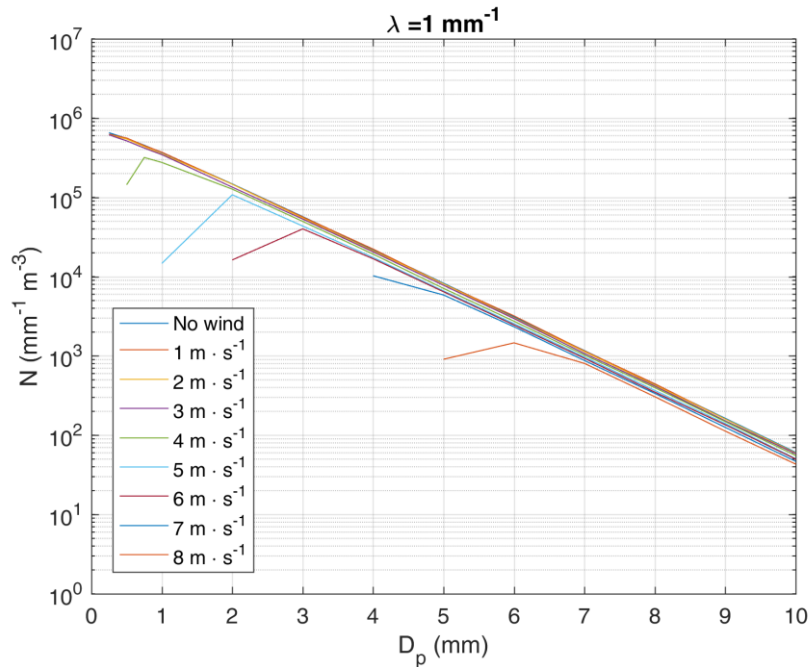
Figure 9: CFD simulated PSD of dry snow collected by the SA shielded gauge under different wind conditions using λ=1.0 mm^{-1} and N_0=10^6 mm^{-1}m^{-3}

For larger diameters, the PSD of the precipitation collected by the gauge maintains the same slope λ of the reference and slightly decrease the concentration number N_0 with increasing U_w. The collected $N(D_p)$ values are lower than the reference PSD but maintain the same order of magnitude. An exception is represented by the smaller diameter of the PSDs collected under wind speeds higher than 4 m s^{-1}. In this case, the $N(D_p)$ value is approximately one order of magnitude lower than the

reference one. The wind-induced underestimation of the SI_{SA} for a given λ is due to the loss of high concentration small particles falling into the gauge.

5.3 Comparing the results of field observations and CFD simulations

The computed *CE* variation with wind speed as a function of *SI* is shown in Figure 10. The results of the CFD trajectory analysis are shown in Figure 10a while the Marshall field site measurements are reported in Figure 10b. The plot is comparable to Figure 8 of Colli et al (2015) where the correlation between the simulated *CE* and the *PSD* was discussed. For any given
10   wind speed, a set of eight *CE* values have been computed according to the slope λ of the reference *PSD*, which is correlated with the *SI* measured by the gauge (equation 1).

The CFD results show that when the wind speed is higher than 3 m s^{-1}, there is an abrupt increase of the *CE* scatter from 1 mm h^{-1}<SI_{SA}<1.5 mm h^{-1} (red points) to 0 mm h^{-1}<SI_{SA}<0.5 mm h^{-1} (blue points), associated with a decrease of the *CE* at a given wind speed (Figure 10a). When the average wind speed is lower or equal to 3 m/s the dependency of the *CE* on the measured
15   *SI* becomes less significant, meaning that even the smaller particles are mostly collected by the SA shielded gauge. The latter result is not confirmed by the field measurements provided in Figure 1 that show a persistent scattering of the *CE* even at the lower wind speeds. Such behaviour has been already explained by Colli et al. (2016b) that demonstrated the role of the airflow turbulence generated by the wind shield in the *CE* scattering by means of time-dependent CFD simulation.

The results of the CFD simulations therefore highlight the physical dependency between the *CE* and the *SI* measured by the
20   gauge, and this dependency varies according to the wind speed. Figure 10b shows the *CE* field observations for the 10-min aggregation interval dataset, categorized by *SI* confirming the dependency between collected precipitation, measured intensity and wind speed.
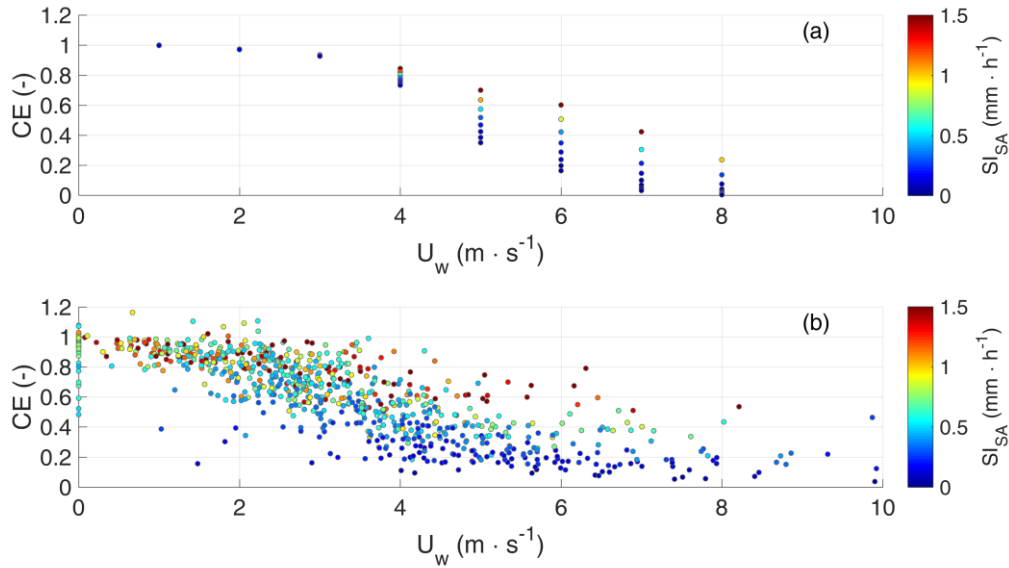
Figure 10: *CE* scatter of the 10-min SA shielded gauge measurements simulated by means of the time-averaged CFD model (panel a) and field measurements (panel b) made at the Marshall field test site (CO, USA). Data are colour coded according to the measured *SI*.

The added value of using the *SI* in the transfer function is best visualised in the SI_{SA} *vs.* SI_{REF} scatter plot shown in Figure 11a, where SI_{REF} is the reference *SI* (assumed coincident with SI_{DFIR} for the field data). In this graph, where the wind speed is colour-coded according to the side bar, the iso-CE lines would be linear (grey dotted lines) in the absence of a clear influence of the SI_{SA} on the *CE*. A clear deviation from linearity is observed, showing that the collection efficiency increases far beyond

10   linearity with the measured *SI* at any wind speed class. This deviation vanishes when $U_w \rightarrow 0$ and increases with the wind speed, therefore justifying the larger spread of *CE* values observed towards the right-hand side of Figure 10 (a and b).
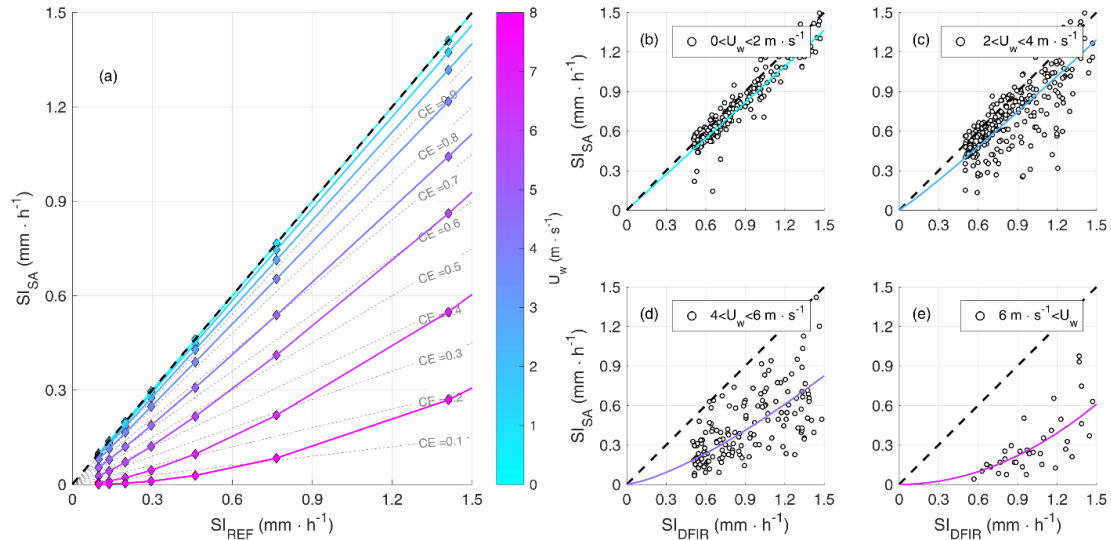
Figure 11: Deviation from linearity of the *CE* (grey dotted lines in (a)) when increasing the wind speed (colour coded according to the side bar) in the measured vs. reference *SI* plane. The deviation is evident in both the results of numerical simulation (solid coloured lines and diamonds in panel a) and field data (white circles in panels b, c, d, e) although with some residual scatter. The field data is presented together with power law regressions performed for various wind speed classes.

6 Conclusions

The present analysis of recent WMO-SPICE quality controlled 30-min accumulation data from the Marshall field-test site (CO, USA) revealed that the wind-induced undercatch of solid precipitation gauges is best correlated with the measured snowfall intensity, rather than temperature, in addition to wind speed. While the environmental temperature provides general relevant information about whether the precipitation is rain (Auer, 1974), wet or dry snow (Rasmussen et al., 1999) it is not clear how the exact type of solid precipitation can be easily determined in the field. At cold temperatures, which are often associated with dry snow, it is also possible to observe rime particles that would have higher collection efficiency (Thériault et al., 2012). On the other hand, the measured snowfall intensity has the advantage of including information about the PSD (Pruppacher and Klett, 1997). Optimal curve fitting used to derive the transfer function for the GEONOR gauge in a Single Alter shield and in a DFIR configuration indicates that accounting for *SI* indeed reduces the scatter of the residuals.

This result is confirmed by the analysis of data from other field sites, such as CARE (Canada) and Haukeliseter (Norway), and shows a consistent behaviour under different climatological conditions. Recent results from Chubb et al. (2015) found improved under-catch correction for an ETI weighing gauge for data collected in the Snowy Mountains of Australia. This supports our results and suggests that other snow gauges can benefit from this type of adjustment.

The physical basis for the improved parameterisation of the transfer function by using the measured *SI* was shown through CFD modelling of the gauge snow collection process to be due to the correlation of large particles with high intensities. Large particles are preferentially collected by a snow gauge, even in strong wind, due to their higher fall velocity, allowing them to

break through streamlines of flow above the gauge and be collected. The CFD modelling was able to reproduce the *CE* pattern observed in the field providing strong evidence of the hypothesized behaviour.

The analysis of the optimal aggregation interval of snowfall measurements was based on the evaluation of the residual data scattering after applying adjustments based on wind speed and either environmental temperature or the measured *SI*. It has been observed that shorter accumulation intervals increase the dependency of the *CE* on *SI* and a stronger benefit in using the proposed approach. On the other hand, it was also observed that larger accumulation intervals are generally associated with a smaller residual scattering of the measurements. According to our analysis, the 10-min aggregation interval may represent a trade-off point between the availability of correlated *SI* and *CE* observations and the need of accumulating significant amounts of snowfall when lower precipitation intensities occur.

Overall, these findings provide an attractive method to improve operational measurements since no additional instrument, except for a wind sensor, is required to derive the adjusted estimates of snow accumulation.

Acknowledgements

J.M Thériault was funded by the Natural Sciences and Engineering Research Council (NSERC) of Canada.

References

Alter, J.: Shielded storage precipitation gages. Mon. Wea. Rev., 65, 262–265, 1937.

Auer, A. H.: The rain versus snow threshold temperature. Weatherwise, 27, 67 (2), 1974.

Brandes, E. A., Ikeda, K., Zhang, G., Schönhuber, M., & Rasmussen, R. M.: A statistical and physical description of hydrometeor distributions in Colorado snowstorms using a video disdrometer. Journal of applied meteorology and climatology, 46(5), 634-650, 2007.

Buisán, S. T., Earle, M. E., Collado, J. L., Kochendorfer, J., Alastrué, J., Wolff, M., Smith, C. D., and López-Moreno, J. I.: Assessment of snowfall accumulation underestimation by tipping bucket gauges in the Spanish operational network, Atmos. Meas. Tech., 10, 1079-1091, 2016.

Chubb, T., M.J. Manton, S.T. Siems, A.D. Peace, and Bilish, S.P.: Estimation of Wind-Induced Losses from a Precipitation Gauge Network in the Australian Snowy Mountains. J. Hydrometeor., 16, 2619–2638, 2015.

Colli, M., R. Rasmussen, J.M. Thériault, L.G. Lanza, C.B. Baker, and Kochendorfer J.: An Improved Trajectory Model to Evaluate the Collection Performance of Snow Gauges. J. Appl. Meteor. Climatol., 54, 1826–1836, 2015.

Colli, M., Lanza, L.G., Rasmussen, R.M. and Thériault, J.M.: The collection efficiency of shielded and unshielded precipitation gauges. Part I: CFD airflow modelling. J. of Hydrometeorol., 17(1), pages 231-243, 2016a.

Colli, M., Lanza, L.G., Rasmussen, R.M. and Thériault, J.M.: The collection efficiency of shielded and unshielded precipitation gauges. Part II: modelling particle trajectories. J. of Hydrometeorol., 17(1), 245-255, 2016b.

Constantinescu, S., Krajewski, W., Ozdemir, C., Tokyay, T.: Simulation of flow around raingauges: Comparison of LES with RANS models. Journal of Advances in Water Resources 30, 43–58, 2006.

5   Eldred, M.S., Agarwal, H., Perez, V.M., Wojtkiewicz, S.F., Jr., and Renaud, J.E.: Investigation of Reliability Method Formulations in DAKOTA/UQ, Structure & Infrastructure Engineering: Maintenance, Management, Life-Cycle Design & Performance, Vol. 3, No. 3, pp. 199-213, 2007.

Folland, C. K.: Numerical models of the raingauge exposure problem, field experiments and an improved collector design. Q.J.R. Meteorol. Soc., 114: 1485-1516, 1988.

10   Gergely M. and Garrett,T.J.: Impact of the natural variability in snowflake diameter, aspect ratio, and orientation on modeled snowfall radar reflectivity. J. Geophys. Research, 121(20), 12,236-12,252, 2016.

Goodison, B., P. Louie, and Yang, D.: WMO solid precipitation measurement intercomparison: final report. WMO Tech. Document 872, World Meteorological Organization, Geneva, Switzerland, 1998.

Houze, R. A., P. V. Hobbs, and Herzegh,P.H.: Size distributions of precipitation particles in frontal clouds. J. Atmos. Sci.,
15   36, 156–162, 1979.

Kochendorfer, J., Rasmussen, R., Wolff, M., Baker, B., Hall, M. E., Meyers, T., Landolt, S., Jachcik, A., Isaksen, K., Brækkan, R., and Leeper, R.: The quantification and correction of wind-induced precipitation measurement errors, Hydrol. Earth Syst. Sci., 21, 1973-1989, 2017a.

Kochendorfer, J., Nitu, R., Wolff, M., Mekis, E., Rasmussen, R., Baker, B., Earle, M. E., Reverdin, A., Wong, K., Smith,
20   C. D., Yang, D., Roulet, Y.-A., Buisan, S., Laine, T., Lee, G., Aceituno, J. L. C., Alastrué, J., Isaksen, K., Meyers, T., Brækkan, R., Landolt, S., Jachcik, A., and Poikonen, A.: Analysis of single-Alter-shielded and unshielded measurements of mixed and solid precipitation from WMO-SPICE, Hydrol. Earth Syst. Sci., 21, 3525-3542, 2017b.

Kochendorfer, J., Nitu, R., Wolff, M., E. Mekis, R. Rasmussen, B. Baker and others: Testing and Development of Transfer Functions for Weighing Precipitation Gauges in WMO-SPICE. Journal of Hydrology and Earth System Sciences
25   Discussions, 2017, 1-25, 2017c.

Matrosov, S.Y., C. Campbell, D. Kingsmill, and E. Sukovich: Assessing Snowfall Rates from X-Band Radar Reflectivity Measurements. J. Atmos. Oceanic Technol., 26, 2324–2339, 2009.

Marshall, J.S. and W.M. Palmer: The distribution of raindrops with size. J. Meteor., 5, 165–166, 1948.

Nespor, V., and B. Sevruk: Estimation of wind-induced error of rainfall gauge measurements using a numerical simulation.
30   J. Atmos. Oceanic Technol., 16 (4), 450–464, 1999.

Nitu, R., Rasmussen, R., Baker, B., Lanzinger, E., Joe, P., Yang, D., Smith, C., Roulet, Y.A., Goodison, B., Liang, H., Sabatini, F., Kochendorfer, J., Wolff, M., Hendrikx, J., Vuerich, E., Lanza, L.G., Aulamo, O., Vuglinsky, V.: WMO intercomparison of instruments and methods for the measurement of solid precipitation and snow on the ground: Organization of the experiment. Preprints, TECO-2012: WMO Technical Conference on Meteorological and
35   Environmental Instruments and Methods of Observations, Brussels, Belgium,WMO,10 pp., 2012.

Nitu, R., Roulet, Y.A., Wolff, M., Earle, M., Reverdin, A., C. Smith, C., Kochendorfer, J., Morin, S., Rasmussen, R., Wong, K., Alastrué, J., Arnold, L., Baker, B., Buisán, S., Collado, J.L., Colli, M., Collins, B., Gaydos, A., Hannula, H.-R., Hoover, J., Joe, P., Kontu, A. Laine, T., Lanza, L., Lanzinger, E., Lee, G.W., Lejeune, Y., Leppänen, L., Mekis, E.,

Panel, J.-M., Poikonen, A., Ryu, S., Sabatini, F., Thériault, J., Yang, D., Genthon, C., van den Heuvel, F., Hirasawa, N., Konishi, H., Nishimura, K., Senese, A.: WMO Solid Precipitation Intercomparison Experiment (SPICE) (2012 - 2015), Instruments and Observing Methods Report No. 131, 2018.

Pruppacher, H.R. and Klett J.D.: Microphysics of Clouds and Precipitation, Atmospheric and Oceanographic Sciences Library, Springer Netherlands, 954 pp., 2010.

Rasmussen, R.M., J. Vivekanandan, J. Cole, B. Myers, and Masters C.: The Estimation of Snowfall Rate Using Visibility. J. Appl. Meteor., 38, 1542–1563, 1999.

Rasmussen, R., B. Baker, J. Kochendorfer, T. Meyers, S. Landolt, A.P. Fischer, J. Black, J.M. Thériault, P. Kucera, D. Gochis, C. Smith, R. Nitu, M. Hall, K. Ikeda, and Gutmann E.: How well are we measuring snow: The NOAA/FAA/NCAR winter precipitation test bed. Bull. Amer. Meteor. Soc., 93, 811–829, 2012.

Reverdin, A.: Description of the Quality Control and Event Selection Procedures used within the WMO-SPICE project, Madrid, Spain, September, 2016.

Thériault, J., Rasmussen, R., Ikeda, K., Landolt, S.: Dependence of snow gauge collection efficiency on snowflake characteristics. Journal of Applied Meteorology and Climatology 51, 745–762, 2012.

Thériault, J.M., R. Rasmussen, E. Petro, J. Trépanier, M. Colli, and Lanza,L.G.: Impact of Wind Direction, Wind Speed, and Particle Characteristics on the Collection Efficiency of the Double Fence Intercomparison Reference. J. Appl. Meteor. Climatol., 54, 1918–1930, 2015.

Thom, A. S.: Momentum, mass and heat exchange of plant communities, in: Vegetation and the Atmosphere, Vol. 1, edited by: Monteith, J. L., Academic Press, London, 1975.

Wolff, M., K. Isaksen, A. Petersen-Øverleir, K. Ødemark, T. Reitan, and Bækkan R.: Derivation of a new continuous adjustment function for correcting wind-induced loss of solid precipitation: results of a norwegian field study. Hydrol. Earth Syst. Sci., 9(11), 10 043–10 084, 2014.

WMO: Guide to Meteorological Instruments and Methods of Observation, World Meteorological Organization Pub. N. 8, 2014 (updated 2017), ISBN 978-92-63-10008-5.

Yang, D., and Goodison, B. E., Metcalfe, J. R., Louie, P., Leavesley, G., Emerson, D., Hanson, C. L., Golubev, V. S., Elomaa, E., Gunther, T., Pangburn, T., Kang, E. and Milkovic, J.: Quantification of precipitation measurement discontinuity induced by wind shields on national gauges. Water Resour. Res., 35 (2), 491508, 1999.